

1 **Chromatographic phospholipid trapping for automated H/D**
2 **exchange mass spectrometry analysis of membrane protein-lipid**
3 **assemblies**

4
5
6
7 **Authors**

8 Dietmar Hammerschmid*, Valeria Calvaresi, Chloe Bailey, Benjamin Russell Lewis, Argyris Politis, Mike
9 Morris, Laetitia Denbigh, Malcolm Anderson, Eamonn Reading*

10
11
12
13 **Corresponding Authors**

14 **Dietmar Hammerschmid** – Department of Chemistry, King’s College London, 7 Trinity Street, SE1 1DB
15 London, UK; orcid.org/0000-0002-0210-3690; Email: dietmar.hammerschmid@kcl.ac.uk

16 **Eamonn Reading** – Department of Chemistry, King’s College London, 7 Trinity Street, SE1 1DB
17 London, UK; orcid.org/0000-0001-8219-0052; Email: eamonn.reading@kcl.ac.uk

18
19 **Authors**

20 **Valeria Calvaresi** – Department of Chemistry, King’s College London, 7 Trinity Street, SE1 1DB London,
21 UK; orcid.org/0000-0002-1756-8853

22 **Chloe Bailey** – Department of Chemistry, King’s College London, 7 Trinity Street, SE1 1DB London,
23 UK; orcid.org/0000-0003-1750-5788

24 **Benjamin Russell Lewis** – Department of Chemistry, King’s College London, 7 Trinity Street, SE1 1DB
25 London, UK; orcid.org/0000-0002-0248-6177

26 **Argyris Politis** – Department of Chemistry, King’s College London, 7 Trinity Street, SE1 1DB London,
27 UK; orcid.org/0000-0002-6658-3224

28 Present address, School of Biological Sciences, The University of Manchester, Oxford Road, M13 9PTUK
29 Manchester M13 9PT, UK, Manchester Institute of Biotechnology, The University of Manchester, Princess
30 Street, M1 7DN Manchester, UK

31 **Mike Morris** – Waters Corporation, Stamford Avenue, Altrincham Road, SK9 4AX Wilmslow, UK

32 **Laetitia Denbigh** – Waters Corporation, Stamford Avenue, Altrincham Road, SK9 4AX Wilmslow, UK

33 **Malcolm Anderson** – Waters Corporation, Stamford Avenue, Altrincham Road, SK9 4AX Wilmslow, UK
34
35

36 **Abstract**

37 Lipid interactions modulate the function, folding, structure, and organization of membrane proteins.
38 Hydrogen/deuterium exchange mass spectrometry (HDX-MS) has emerged as a useful tool to understand
39 the structural dynamics of these proteins within lipid environments. Lipids, however, have proven
40 problematic for HDX-MS analysis of membrane-embedded proteins, due to their presence impairing
41 proteolytic digestion, causing liquid chromatography column fouling, ion suppression, and/or mass spectral
42 overlap. Here, we describe the integration of a chromatographic phospholipid trap column into the HDX-
43 MS apparatus to enable online sample delipidation prior to protease digestion of deuterium labeled protein-
44 lipid assemblies. We demonstrate the utility of this method on membrane scaffold protein lipid nanodisc –
45 both empty and loaded with the ~115 kDa transmembrane protein AcrB – proving efficient and automated
46 phospholipid capture with minimal D-to-H back-exchange, peptide carry-over, and with minimal protein
47 loss. Our results provide insights into the efficiency of phospholipid capture by ZrO₂-coated and TiO₂
48 beads, and describe how solution conditions can be optimized to maximize the performance of our online,
49 but also the existing offline, delipidation workflows for HDX-MS. We envision that this HDX-MS method
50 will significantly ease membrane protein analysis, allowing to better interrogate their dynamics in artificial
51 lipid bilayers or even cell membranes.

52

53

54 **Introduction**

55 Membrane proteins have an intimate relationship with their surrounding lipid bilayer^[1-5]. The amphipathic
56 nature of the lipid bilayer combined with the high degree of hydrophobicity possessed by membrane
57 proteins makes their study significantly more difficult compared to their soluble protein counterparts. To
58 interrogate these systems, new analytical tools are required; the importance of this endeavor being
59 intensified by the fact that membrane proteins are key targets for more than half of modern drugs^[6].

60
61 Protocols have been established to enable hydrogen/deuterium exchange mass spectrometry (HDX-MS)
62 analysis of membrane proteins within lipid vesicles^[7], liposomes^[8], nanodiscs^[9-12] and so-called ‘native
63 nanodiscs’, which allow membrane proteins to stay in contact with the native lipid milieu^[5,13,14]. In HDX-
64 MS, a protein is diluted into a deuterated buffer enabling H/D exchange of its labile backbone amide
65 hydrogens. This reaction is quenched at different time intervals by dropping pH and temperature to 2.5
66 and 0 °C, respectively. The quenched protein sample is then digested by an acid-labile protease (e.g. pepsin)
67 into peptides and the incorporation of deuterium measured by liquid chromatography (LC)-MS analysis.
68 Post deuterium labeling, however, lipids can cause manifold issues in the bottom-up HDX-MS workflow^[15].
69 These problems range from a reduced protein digestion efficiency due to potential interference with the
70 protease, to fouling of the liquid chromatography system, peptide-lipid co-elution that adds to spectral
71 complexity, and peptide ion suppression.

72
73 The addition of ZrO₂-coated beads post deuterium labeling offers a sophisticated strategy for depriving the
74 protein samples of lipid components under HDX quench conditions^[16]. Yet, beads need to be removed
75 through filtration before sample injection into the mass spectrometer, which is laborious and time
76 consuming, thus, may affect reproducibility among technical replicates and inevitably increases the D-to-H
77 back-exchange^[17-20]. This process has recently been automated for HDX-MS applications: Anderson et al^[21]
78 developed a robot-assisted workflow with nanofilter vials, where the labeled protein is transferred to the
79 base of a filter system containing ZrO₂ beads, and after binding of phospholipids, the sample is filtered
80 through a nanofilter cartridge by a LEAP X-Press module harvesting the protein for subsequent injection.
81 The ZrO₂ beads and cartridge are then disposed after each experiment. Other approaches for phospholipid
82 removal that avoid the use of ZrO₂ beads have also been developed, including TCA precipitation^[7] and the
83 use of size-exclusion chromatography (SEC)^[22]. Here, we report an alternative chromatographic approach
84 which enables online, regeneratable phospholipid trapping by a ZrO₂ bead column. This exploits the Lewis
85 acid chemistry of ZrO₂ - whilst avoiding the need for precipitation, size separation, filtration or bead
86 disposal - to offer a robust automated system for HDX, digestion and LC-MS analysis of proteins within
87 lipid environments.

88
89 We determined crucial parameters, such as delipidation efficiency, system robustness, and back-exchange
90 levels, and minimized unspecific protein/peptide adsorption to the column matrix. We also investigated

91 titanium oxide (TiO_2) beads as an alternative to ZrO_2 -based protein delipidation. Furthermore, we
92 established an automated wash method for bead regeneration in parallel to peptide LC-MS analysis, which
93 enables intervention-free sample acquisition and makes the phospholipid trap column reusable. Finally, we
94 demonstrated the functionality of the delipidation protocol by HDX-MS analysis of empty and loaded
95 membrane scaffold protein phospholipid nanodiscs, the latter loaded examples containing multidrug efflux
96 pump transmembrane subunit AcrB. We envision that this automated and robust delipidation workflow
97 will make HDX-MS analysis of membrane-embedded proteins routine.

98

99

100 **Experimental Section**

101 **Materials**

102 Zirconia (ZrO₂) coated silica bulk (Cat No. 5425-U) was purchased from Supelco. Titansphere (TiO₂) 100 Å
103 5 μm, bulk, (Cat No. GL-5020-75000) was purchased from GL Sciences. 1-palmitoyl-2-oleoyl-sn-glycero-
104 3-phosphocholine (POPC; Cat No. 850457) and E. coli Total Lipid Extract (EPL; Cat No. 100500) were
105 purchased from Avanti Polar Lipids. N-Dodecylphosphocholine (Fos-choline-12; Cat No. F308S) and n-
106 Dodecyl-β-D-Maltopyranoside (DDM; Cat No. D310) were purchased from Anatrace. Phosphorylase b
107 (PhosB) from rabbit muscle (Cat No. P6635), Bovine Serum Albumin (BSA; Cat No. A2153), Deuterium
108 oxide (99.9 atom%D; Cat No. 151882), Ammonium hydroxide (Cat No. 221228), 2,5-Dihydroxybenzoic
109 acid (Cat No. 149357), and DL-Lactic acid (Cat No. 69785) were purchased from Sigma-Aldrich. Water
110 (Optima™ LC/MS grade; Cat No. W61), Acetonitrile (Optima™ LC/MS grade; Cat No. A9551), Methanol
111 (Optima™ LC/MS grade; Cat No. A4561), Isopropanol (Optima™ LC/MS grade; Cat No. A4611), and
112 Formic acid (99.0+%, Optima™ LC/MS grade; Cat No. A11750) were purchased from Fisher Scientific.
113 Guanidinium hydrochloride (Cat No. 0118) and glycine (Cat No. 1504) were purchased from VWR Life
114 Sciences. Potassium phosphate monobasic (Cat No. 094578) and dibasic (Cat No. 094672) were purchased
115 from Flourochem.

116

117 **Instrumentation (Standard HDX)**

118 All experiments were performed on an ultraperformance liquid chromatography (UPLC) system
119 (nanoACQUITY, Waters, Wilmslow, UK) coupled to an electrospray ionization quadrupole time-of-flight
120 (ESI-Q-ToF) mass spectrometer (Xevo G2-XS, Waters, Wilmslow, UK). The standard nanoACQUITY
121 system contains a refrigerated HDX manager with a two-valve configuration, i.e. injection and trapping
122 valve, supplies solvent flow via Auxiliary (ASM) and Binary (BSM) Solvent Managers. The HDX manager
123 was kept at 0 °C during all measurements.

124

125 **Delipidation Setup (Extended HDX)**

126 The standard configuration was extended by an additional 'delipidation' valve which was positioned
127 between injection and trapping valve (**Figure 1**). The delipidation valve was equipped with an in-house
128 packed phospholipid trap column (ZrO₂ or TiO₂), which was kept on ice (**Figure S1C**).

129

130 **Column Packing**

131 Columns for chromatographic phospholipid trap column (ZrO₂ or TiO₂ beads) and protein digestion
132 (Pepsin agarose resin, Cat No. 20343; Thermo Fisher) were packed in-house using both a Microbore Guard
133 Column (1.0 mm ID x 2 cm unpacked; Part No. C-128) and an Analytical Guard Column (2.0 mm ID x 2
134 cm unpacked; Part No. C-130B) from UVISION Technologies (London, UK). Beads were resuspended
135 and washed in solvent A (0.23% formic acid in H₂O, pH 2.5). Column parts were cleaned by sonication in
136 solvent A. The column was assembled without the frit (**Figure S1B**) on the side from which the column

137 was packed using a syringe with an appropriate adapter. After packing, the missing frit was inserted, and
138 the column was flushed back-to-back with solvent A by applying a constant pressure with the ASM for a
139 couple of minutes, allowing the bead matrix to settle.

140

141 **Lipid Preparation**

142 POPC and EPL (composition: 67.0% phosphatidylethanolamine, 23.2% phosphatidylglycerol, 9.8%
143 cardiolipin) lipids were dissolved in cyclohexane and transferred into a glass vial. Cyclohexane was
144 evaporated under a gentle N₂ stream. The dried lipid film was flash frozen in liquid N₂ and further freeze-
145 dried for five hours. Lipids were resuspended (5 mg/mL) in 10 mM potassium phosphate buffer (pH 7.0)
146 under gentle agitation for 1 hour, followed by sonication for 1 hour. Fos-choline-12 (5 mg/mL) was
147 solubilized in solvent A. Before injection, lipids were diluted to the appropriate concentration and finally
148 added to ice-cold 100 mM potassium phosphate buffer, pH 2.3 (1:1 vol/vol; final pH 2.5).

149

150 **Preparation of MSP1E3D1 scaffold protein**

151 pMSP1E3D1 containing "extended" MSP1D1 (Addgene) - which contains repeats of helices 4, 5 and 6, an
152 N-terminal 7-his tag followed by spacer sequence and TEV protease cleavage site – was overexpressed in
153 *E. coli* BL21(DE3) cells as described previously^[23,24]. Cells were resuspended in lysis buffer (20 mM Na-
154 phosphate, pH 8.0, 1% Triton X-100, 10 µg/ml DNAase, 1 mM PMSF, and a protease inhibitor tablet)
155 and sonicated on ice applying 3 x 10 second pulses with 30 seconds breaks. Cell lysate was centrifuged at
156 25,000 x g for 30 minutes. The supernatant was mixed with 4 ml of Ni-NTA Superaffinity resin and
157 incubated for 1 hour at room temperature under gentle agitation. The resin was loaded into a pre-chilled
158 Biorad polyprep column for subsequent purification at 4 °C. The resin was washed with 10 column volumes
159 (CVs) of wash buffer A (40 mM Tris-HCl, 300 mM NaCl, 1% Triton X-100, pH 8.0), 10 CVs of wash
160 buffer B (40 mM Tris-HCl, 300 mM NaCl, 50 mM Na-cholate, 20 mM Imidazole, pH 8.0), and finally 10
161 CVs of wash buffer C (40 mM Tris-HCl, 300 mM NaCl, 50 mM Imidazole, pH 8.0). MSP1E3D1 protein
162 was eluted with 5 CVs of elution buffer (40 mM Tris-HCl, 300 mM NaCl, 500 mM Imidazole, pH 8.0).
163 Fractions were tested for purity by SDS-PAGE and the cleanest samples were pooled and dialyzed against
164 MSP buffer (20 mM Tris-HCl, 100 mM NaCl, 0.5 mM EDTA, pH 7.4) at 4 °C. Finally, the sample was
165 filtered using a 0.22 µm membrane, aliquoted, flash frozen with liquid nitrogen and stored at –80 °C.

166

167 **Nanodisc Preparation**

168 Lipid nanodiscs (POPC or EPL) were prepared as previously described^[23,25]. Lipids were re-solubilized with
169 MSP buffer (20 mM Tris-HCl, 100 mM NaCl, 0.5 mM EDTA, pH 7.4) containing 200 mM and 500 mM
170 Na-cholate for POPC and EPL lipids respectively. MSP1E3D1 was added to the resuspended lipids at a
171 1:85 and 1:60 MSP:lipid molar ratio for POPC and EPL lipids respectively. Nanodisc mixtures with lipids,
172 Na-cholate, and MSP were incubated at 4 °C for 30 min. BioBeads SM-2 (Bio-Rad) were added (~0.5 g of
173 beads per 1 mL volume) to remove Na-cholate and drive nanodisc self-assembly. The MSP:lipid:cholate

174 reconstitution was incubated with beads for at least 8 h with at least three bead changes. Beads were
175 removed by filtration and generated nanodiscs were then purified using a Superdex 200 10/300 Increase
176 GL column (GE Healthcare) in MSP buffer (**Figure S2**). Purity and size were assessed by SDS-PAGE and
177 dynamic light scattering (DLS) using a Particle Size Analyzer LiteSizer 500 (Anton Parr).

178

179 **Preparation of AcrB in Nanodiscs**

180 AcrB was purified in DDM as described previously^[26]. After purification, AcrB was inserted into nanodiscs
181 according to the previously established protocols^[23,27]. Briefly, AcrB in 0.03% (w/v) DDM detergent was
182 mixed with POPC and MSP solution at a final 40:1:0.5 lipid:MSP1E3D1:AcrB molar ratio in MSP buffer
183 with final concentration of 0.0116% (w/v) DDM and 16 mM Na-cholate. DDM was removed by the
184 addition of SM2 Bio-beads (Bio-Rad) into the mixture and left in an orbital shaker overnight at 4 °C. AcrB
185 nanodiscs were purified using a Superdex 200 Increase 10/300 (GE Healthcare) in AcrB sample buffer (50
186 mM sodium phosphate, 150 mM NaCl, 10% glycerol, pH 7.4) (**Figure S3**).

187

188 **Lipid Measurements**

189 The HDX manager was equipped with a Vanguard column (BEH C4, 300 Å, 1.7 µm, 2.1 mm x 5 mm;
190 Waters) only. Lipids were trapped on the C4 column and washed with solvent A for 3 minutes at
191 200 µL/min. Subsequently, lipids were eluted by a 3-minute linear gradient from 5 to 95% solvent B (0.23%
192 formic acid in acetonitrile, pH 2.5) at 40 µL/min. Eluted lipids were measured in positive ion mode between
193 50 and 2,000 m/z on the Xevo G2-XS mass spectrometer. The phospholipid trap column was cleaned with
194 3% NH₄OH in methanol and re-equilibrated in solvent A during the subsequent wash run. Experiments
195 were performed in the standard two-valve and extended three-valve HDX-MS configuration. Detailed LC
196 settings are provided in Supporting Information (**Table S1 and S2**). The extracted ion chromatogram (EIC)
197 of the respective lipid was generated and mass spectra were combined at full width half maximum (FWHM).
198 The obtained intensity read was used to calculate the delipidation efficiency of the column/system.

199

200 **Protein Measurements**

201 PhosB was solubilized in equilibration buffer (10 mM potassium phosphate, pH 7.0) and diluted 1:1
202 (vol/vol) with the quench buffer (100 mM potassium phosphate, pH 2.3). The HDX manager of the
203 nanoACQUITY system was equipped with a Vanguard column (BEH C18, 130 Å, 1.7 µm, 2.1 mm x 5
204 mm; Waters) and an Acquity UPLC column (BEH C18, 130 Å, 1.7 µm, 1.0 mm x 100 mm; Waters) for
205 peptide trapping and separation, respectively. Protein digestion was performed online with the UPLC
206 chromatographic system using an in-house packed protease column (immobilized pepsin agarose resin) at
207 15 °C. The generated peptides were trapped and washed with solvent A at 200 µL/min for 3 minutes.
208 Subsequently, peptides were separated by applying a 7.5-minute linear gradient from 8 to 35% solvent B at
209 40 µL/min. Peptides were measured in positive ion mode between 50 and 2,000 m/z on the Xevo G2-XS
210 mass spectrometer. Experiments were performed in triplicates on the standard two-valve and extended

211 three-valve configuration applying standard bottom-up HDX-MS workflow. Detailed LC settings are
212 provided in Supporting Information (**Table S3 and S5**).

213

214 **Evaluation of Back-exchange**

215 PhosB was digested on the in-house packed protease column at a flow rate of 200 $\mu\text{L}/\text{min}$. The generated
216 peptides were collected for 1 minute and subsequently freeze dried for five hours. Peptides were
217 resuspended in deuterated labeling buffer (10 mM potassium phosphate, pH_{read} 6.6; 100% final D_2O
218 content) for four hours. The reaction was quenched by adding 1:1 (vol/vol) ice-cold quench buffer (500
219 mM glycine-HCl, pH 2.35). Measurements were performed in triplicates on both standard two-valve and
220 extended three-valve configuration. Peptide trapping and separation was performed on standard C18 trap
221 and analytical columns at 0 $^\circ\text{C}$. The protease column was replaced by a union and the compartment was
222 kept at 15 $^\circ\text{C}$. The phospholipid trap column was kept on ice. Detailed LC settings are provided in
223 Supporting Information (**Table S3 and S5**).

224

225 **Evaluation of Peptide Carry-over**

226 PhosB was solubilized in equilibration buffer (10 mM potassium phosphate, pH 7.0) and diluted 1:1
227 (vol/vol) by the addition of ice-cold quench buffer (500 mM glycine-HCl, pH 2.35). Measurements were
228 performed in three subsequent runs with a standard wash runs, i.e. pepsin wash (1.6 M guanidinium-HCl,
229 4% acetonitrile, 0.8% formic acid), in between. Then, a blank run (1:1 mix of equilibration and quench
230 buffer) was performed and carry-over was evaluated based on peptide intensities. Detailed LC settings are
231 provided in Supporting Information (**Table S3 and S5**).

232

233 **H/D Exchange Mass Spectrometry of Empty MSP1E3D1 Nanodisc**

234 The extended HDX valve configuration was used and equipped with a ZrO_2 -packed phospholipid trap
235 column (kept on ice) upstream an in-house packed pepsin column (kept at 15 $^\circ\text{C}$). The HDX manager was
236 equipped with a Vanguard column (BEH C18, 130 \AA , 1.7 μm , 2.1 mm x 5 mm; Waters) and an Acquity
237 UPLC column (BEH C18, 130 \AA , 1.7 μm , 1.0 mm x 100 mm; Waters) for peptide trapping and separation,
238 respectively. Deuterium labeling was performed with a PAL3 RTC HDX robot (Trajan Scientific,
239 Morrisville, US). MSP1E3D1 nanodiscs, both POPC (1:85 protein:lipid) and EPL (1:60 protein:lipid), were
240 diluted 20-fold (95% D_2O final) into deuterated labeling buffer (20 mM Tris, 100 mM NaCl, 0.5 mM
241 EDTA, pH_{read} 7.0) for 10, 100, 1,000, and 10,000 seconds at 20 $^\circ\text{C}$. References were performed in non-
242 deuterated equilibration buffer. The reaction was quenched by adding 1:1 (vol/vol) ice-cold nanodisc
243 quench buffer (500 mM glycine-HCl, 1.6 M guanidinium-HCl, 0.8 mM Na-cholate, pH 2.35). Three
244 technical replicates were performed with standard bottom-up HDX-MS workflow applying a 7.5-minute
245 linear gradient from 8 to 35% solvent B at 40 $\mu\text{L}/\text{min}$. Peptides were measured in positive ion mode
246 between 50 and 2,000 m/z on the Xevo G2-XS mass spectrometer, applying settings to minimize gas-phase
247 back-exchange^[28]. The phospholipid trap column was cleaned with 3% NH_4OH in methanol and re-

248 equilibrated in solvent A during the subsequent wash run. Labeling experiments were also performed on
249 free soluble MSP1E3D1 (95% D₂O for 10, 100, 1,000, and 10,000 sec), which was measured on both
250 standard two- and extended three-valve configuration. Detailed LC settings are provided in Supporting
251 Information (**Table S3 and S5**).

252

253 **Mass Spectrometry of AcrB Nanodiscs**

254 AcrB nanodiscs were equilibrated in non-deuterated AcrB sample buffer (no D₂O labeling performed) and
255 ice-cold nanodisc quench buffer was added 1:1 (vol/vol). Three technical replicates were performed with
256 standard bottom-up HDX-MS workflow applying a 9.0-minute linear gradient from 8 to 40% solvent B at
257 40 μ L/min (**Figure S14**). The total protein amount injected was 20 pmol. Detailed LC settings are provided
258 in Supporting Information (**Table S4 and S5**).

259

260 **Data Processing**

261 Lipid spectra were processed with MassLynx 4.2 (Waters, Wilmslow, UK). Protein identification (PhosB
262 and MSP1E3D1) and peptide filtering were performed with ProteinLynx Global Server 3.0 (PLGS) and
263 DynamX 3.0, respectively (Waters, Wilmslow, UK). PLGS workflow parameters for peptide identification
264 were: peptide tolerance: automatic; fragment tolerance: automatic; min fragment ion matches per peptide:
265 2; minimum fragmentation matches per protein: 7; minimum peptide matches per protein: 3; maximum
266 protein mass 250,000; primary digest reagent: non-specific; false discovery rate: 100. DynamX parameters
267 for peptide filtering were: minimum intensity: 1481; minimum sequence length: 5; maximum sequence
268 length: 25; minimum products per amino acid: 0.11; minimum consecutive products: 1; minimum score:
269 6.62; maximum MH⁺ error (ppm): 5; file threshold: $n-1$ ^[29]. Bimodal isotopic envelope analysis was
270 performed with HX-Express2 on the MSP1E3D1 peptide WDNLEKETEGLRQEMSKD, after spectra
271 were smoothed 4 x 2 using Savitzky-Golay in MassLynx^[30].

272

273

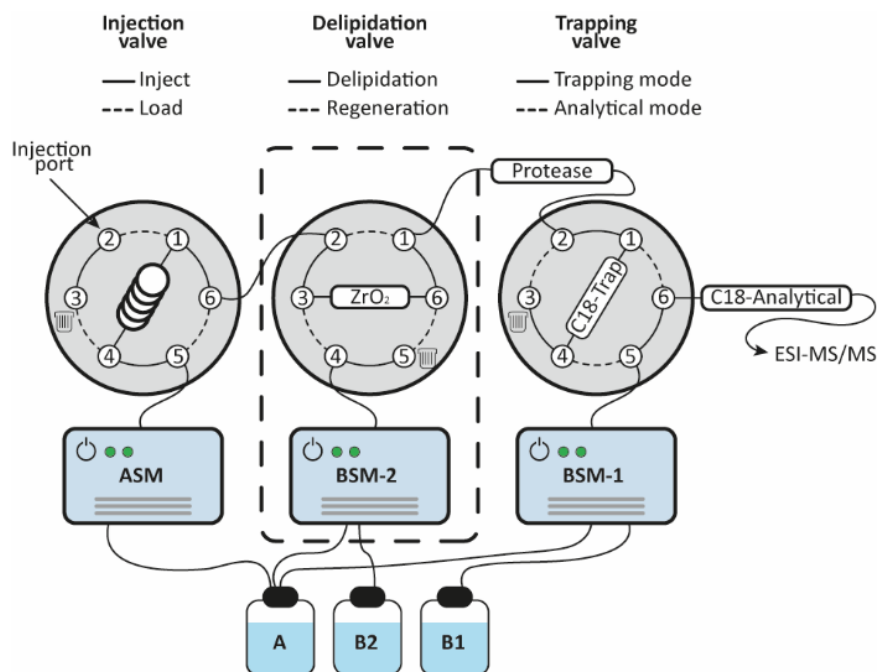
274 **Results and Discussion**

275 **Automated Phospholipid Trapping**

276 Automation endeavors always aim for both repeatability – ideally free of user interventions – and system
277 robustness. To meet these requirements for the automated trapping of phospholipids in HDX-MS
278 experiments, we integrated an additional valve online with the chromatographic system but placed outside
279 the standard two-valve Waters HDX chamber, conventionally used for standard bottom-up HDX-MS
280 analysis (**Figure 1**). The delipidation valve is equipped with a phospholipid trap column, which is kept
281 refrigerated in a polystyrene box containing ice (0 °C) and supplied with eluents by an additional binary
282 solvent manager (BSM) to provide independence from standard HDX-MS solvents. The three-valve system
283 is of straightforward use and fully automated (in our case, controlled by the Waters MassLynx software),
284 and can be coupled to a robot performing automated deuterium labeling and sample injection.

285
286 The developed online delipidation method - with integrated phospholipid trap - works as follows. 1) After
287 the sample injection, the sample components are fed by an auxiliary solvent manager (ASM) through the
288 phospholipid trap column, where lipids are retained, while the protein passes through. 2) The protein is
289 further guided to the online protease column for digestion, and generated peptides are captured in the
290 peptide trap column for desalting. 3) At the end of the trapping time, the phospholipid trap column is
291 automatically configured off-line with the protease column. While the latter can be selectively flushed with
292 a protease wash solution, the phospholipid trap column is washed with an alternate solvent (which we
293 denote as solvent B2) for removal of retained phospholipids, which are directed to a waste compartment.
294 The cleaning step (regeneration) of the phospholipid trap column occurs simultaneously to LC peptide
295 separation, thus with no extra-time added to the sample run. 4) In conventional HDX-MS measurements,
296 following each protein sample run, the analytical segments are usually washed with a sawtooth-gradient run.
297 In the three-valve system, during this wash run, the phospholipid trap column remains configured off-line
298 from the protease column and is re-equilibrated with solvent A (typically 0.23% formic acid), preparing it
299 for the subsequent sample injection. The three-valve configuration also provides flexibility, as the
300 phospholipid trap column can be positioned up- or downstream the protease column, allowing sample
301 delipidation to be performed at protein or peptide level, respectively, without requiring further
302 modifications on the LC methods.

303



304

305 **Figure 1: Schematic illustration of the automated phospholipid trapping workflow.** The conventional two-valve
 306 configuration in standard HDX-MS is extended by an additional valve (dashed box) flanked by injection and trapping
 307 valve. The delipidation valve is equipped with a phospholipid trap column and operated by an extra BSM to provide
 308 independence from standard HDX-MS solvents. In this configuration, the sample passes through the phospholipid
 309 trap column where lipids are retained, and the protein is transported further to the protease column following the
 310 standard bottom-up workflow of protein digestion, peptide trapping, and subsequent analysis. After delipidation and
 311 protein digestion, the ZrO_2 column can be cleaned simultaneously to peptide analysis using the BSM-2.

312

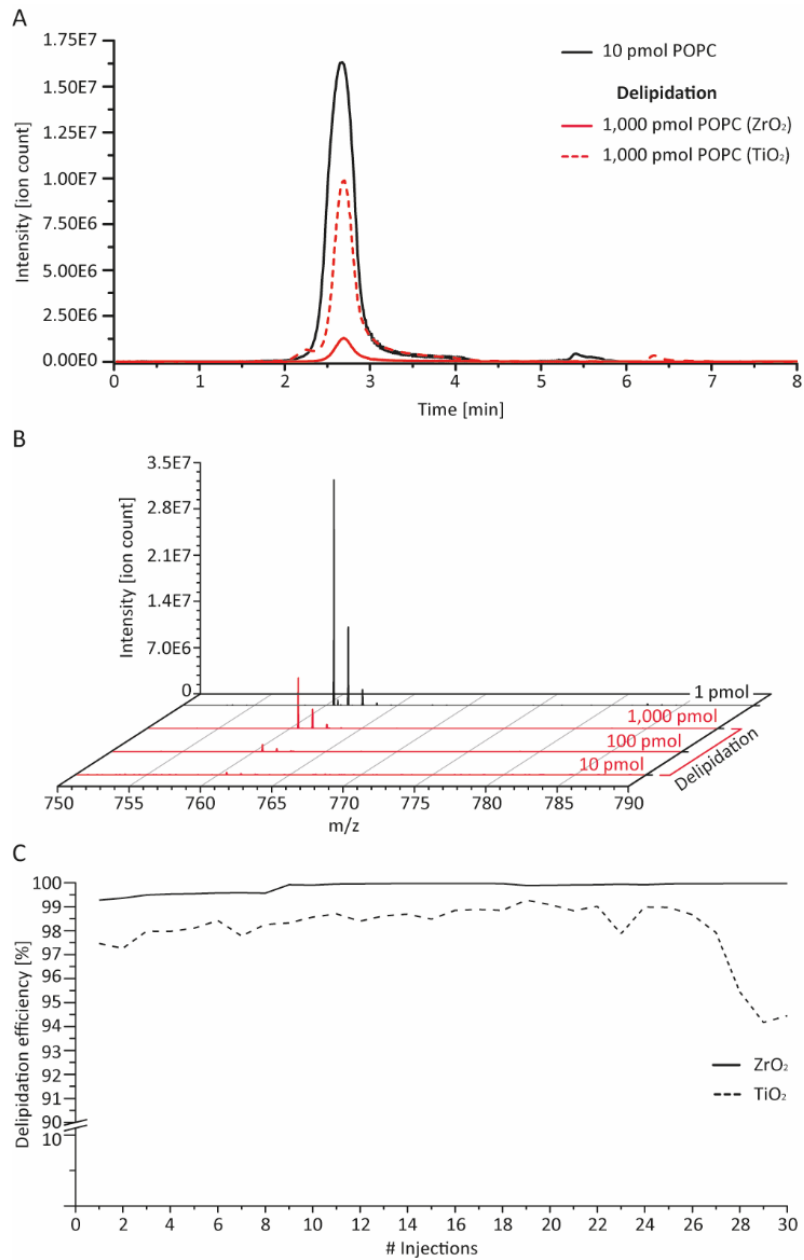
313 **Determining the Delipidation Efficiency**

314 To investigate whether phospholipids are retained after passing through the phospholipid trap column, we
 315 measured lipids on both the standard two-valve and the extended three-valve HDX-MS system. Initially,
 316 we injected four 1-palmitoyl-2-oleoyl-sn-glycero-3-phosphocholine (POPC) aggregates (0.01, 0.1, 1, and 10
 317 pmol) in duplicates and plotted the obtained MS signal against the amount of lipid (**Figure S4A**). After
 318 that, we increased the concentration of POPC and ran triplicates over the delipidation system (three-valve
 319 configuration), applying both the ZrO_2 and the TiO_2 column. The remaining POPC signal after
 320 phospholipid trapping was used to calculate the delipidation efficiencies for the applied column/system.

321

322 The extracted ion chromatogram (EIC) as well as the MS signal of POPC impressively illustrates a >100-
 323 1,000-fold lipid reduction for both bead types, with ZrO_2 outperforming TiO_2 (**Figure 2A, 2B**). We
 324 performed similar lipid trapping experiments applying an *Escherichia coli* lipid extract (EPL) and Fos-choline-
 325 12. Again, we plotted the intensity of the lipid signal against the injected amount (**Figure S4B, S4C**) and
 326 exploited the remaining MS signal to calculate the system's delipidation capacity (**Table 1, S6, S7; Figure**
 327 **S5**). For EPL, we determined lipid removal efficiency for each lipid individually, which is ~96% for ZrO_2
 328 and ~87% for TiO_2 , slightly lower than for POPC (**Table 1, S6, S7**). Both bead types, however, do not

329 show any discrimination in terms of lipid length (**Figure S6**). In standard HDX-MS analysis of membrane
330 proteins, detergents are usually added to the quench buffer to facilitate nanodisc rupture^[10,13]. Hence, we
331 also determined the delipidation capacity in presence of detergents, e.g. 0.1% DDM or 0.1% Fos-choline-
332 12 (a concentration above their critical micelle concentration). DDM causes a significant drop of the
333 delipidation efficiency (32% and 60% of POPC removal for ZrO₂ and TiO₂ respectively, **Table 1**),
334 potentially due to steric hindrance through a bigger micelle formation. However, Fos-choline-12 exerts no
335 detrimental effect in terms of measured lipid removal. Moreover, despite structural similarities with
336 phospholipids, i.e. the phosphatidylcholine headgroup, TiO₂ fails to retain Fos-choline-12, while ZrO₂
337 shows an even stronger binding than for POPC (**Table 1; Figure S5**). Therefore, while the presence of
338 DDM in the quench buffer appears disadvantageous, Fos-choline-12 appears highly suitable as delipidation-
339 compatible quench buffer additive, as ZrO₂ beads also prevent the disadvantageous Fos-choline-12
340 contamination of the downstream chromatography and MS source. Current workflows perform the
341 delipidation step offline from the UPLC system^[10,13,21], which greatly differs to the online chromatographic
342 approach presented here. Comparing both approaches in terms of their lipid removal capacity reveals a
343 better performance of the column-based workflow introduced here (**Table 1**), adding another advantage
344 to the automation benefit.
345
346



347

348

Figure 2: Delipidation efficiency and system robustness of the automated phospholipid trapping workflow.

349

(A) Extracted ion chromatogram of POPC (760.6 m/z) before (solid black) and after (ZrO₂: solid red, TiO₂: dashed

350

red) applying online sample delipidation. (B) Mass spectra of various POPC amounts acquired w/o the ZrO₂ trap

351

column in place. (C) Delipidation efficiency of both bead types (ZrO₂: solid line, TiO₂: dashed line) over the course

352

of 30 POPC injections with appropriate column cleaning in between.

353

Lipid/Sample	Column	Lipid amount	Efficiency [%]	
			ZrO ₂	TiO ₂
POPC	2 x 20 mm	10 pmol	99.97 ± 0.01	99.96 ± 0.01
POPC in DDM	2 x 20 mm	10 pmol	31.94 ± 6.92	60.26 ± 1.65
POPC in Fos-choline-12	2 x 20 mm	10 pmol	99.83 ± 0.06	99.71 ± 0.04
EPL (PE 33:1)	2 x 20 mm	10 ng	97.30 ± 0.33	86.90 ± 0.50
Fos-choline-12	2 x 20 mm	100/10 pmol	99.99 ± 0.00	7.39 ± 4.38
POPC	no column (offline)	10 pmol	95.44 ± 0.21	ND
POPC	1 x 20 mm	10 pmol	98.95 ± 0.29	ND
POPC	1 x 20 mm (blocked)	10 pmol	89.03 ± 0.49	ND
POPC(optimized quench buffer)	1 x 20 mm (blocked)	10 pmol	90.59 ± 1.00	ND

354 **Table 1: Delipidation capacity of ZrO₂ and TiO₂.** Overview of delipidation efficiencies of ZrO₂ and TiO₂ beads
355 determined for different column dimensions and a variety of phospholipids w/o the presence of detergents. A detailed
356 overview of all delipidation rates is provided in **Table S6-S8**. ND ≡ not determined.

357

358 Column Regeneration

359 Recurring lipid injections require the phospholipid trap column to be cleaned to retain delipidation capacity
360 over a long period of time. We tested the suitability of different MS-compatible solvents, such as
361 acetonitrile, isopropanol, and methanol, for cleaning the phospholipid trap column. Standard protocols in
362 phosphoproteomics apply an increasing basicity with ammonium hydroxide (NH₄OH) to elute
363 phosphopeptides from TiO₂^[31–35], providing an alternative to organic solvents. To investigate the lipid
364 cleaning capacity of the different solvents, we loaded 1 pmol POPC on the ZrO₂ column and subsequently
365 applied a saw-tooth gradient of 5 x two minutes washes from 0-100% solvent B2 (**Figure S7**). Success, i.e.
366 cleaning of the phospholipid trap column, would not only be indicated by MS detection of the lipid, but
367 also by a decreasing of its signal intensity over the various gradient cycles. Such an EIC profile is displayed
368 for methanol and 3% NH₄OH, which performs even better in combination (**Figure S7**).

369

370 Delipidation System Robustness

371 We investigated the robustness of the entire delipidation system by recurring POPC injections (30
372 injections) with appropriate cleaning (3% NH₄OH in methanol) of the phospholipid trap column, both
373 ZrO₂ and TiO₂, in between. Advantageously, the column regeneration occurs simultaneously to the
374 analytical gradient. The subsequent wash run – a step commonly applied to prevent sample carry-over –
375 was applied to not only clean the C4 trap column but also to re-equilibrate the phospholipid trap column
376 to solvent A (0.23% formic acid), i.e. to pH 2.5. The delipidation efficiency is comparable with previous
377 results (**Table 1**) and, most impressively, remains over 99% for ZrO₂ throughout (**Figure 2C**). The
378 delipidation rates obtained for TiO₂ are slightly lower (~97-98%), yet reasonably sufficient, and show a
379 drop by 3% within the last three injections.

380

381 **ZrO₂/TiO₂ Trap:Protein Interactions**

382 The integration of an additional column into the delipidation system might lead to unfavorable, unspecific
383 interactions between the target protein and the phospholipid trap column matrix. To investigate such
384 unspecific adsorption effects, we conducted bottom-up PhosB measurements on both systems, i.e. standard
385 two-valve and extended three-valve HDX-MS configuration. We solubilized PhosB in 10 mM potassium
386 phosphate (pH 7.0) and diluted it in 100 mM potassium phosphate (pH 2.3), simulating HDX quench
387 conditions (final pH of 2.5 at 0 °C). Then, we compared the peptide intensities obtained before and after
388 passing through the TiO₂ or ZrO₂ column. We measured the extent of unspecific binding of PhoB to the
389 phospholipid trap column on both protein and peptide level, as the phospholipid trap column can be
390 operated up- and downstream the protease column. Unfortunately, the degree of unspecific column:peptide
391 and in particular column:protein interactions were significant (**Figure 3A**), making reliable peptide
392 measurements difficult not to say impossible. Put simply, unspecific adsorption effects are more severe for
393 intact protein than on the peptide level. Only TiO₂:peptide interactions seem to be mostly negligible. On
394 the protein level, the loss in intensity amounts to two orders of magnitude on average independent of the
395 bead type, which decreases the signal-to-noise ratio to an unacceptable degree for most peptides. We also
396 calculated the percentage of detected peptides relative compared to control measurements performed in
397 the two-valve configuration. The loss of identifiable peptides ranges from 15 to 30% on the protein level
398 for both bead types and for the ZrO₂:peptide configuration (**Figure 3A**). Solely the setup for TiO₂:peptide
399 measurements is acceptable in terms of peptide loss. The addition of a chaotropic agent to the quench
400 buffer, e.g. 3.0 M guanidinium-HCl (1.5 M final) as potential suppressor of unspecific protein/peptide
401 adsorption leads to a marginal increase of signal. The number of undetected peptides however remains
402 largely unimproved, accounting still for 15-20%.

403

404 Following this, we intensified our endeavors to prevent unspecific adsorption to the column matrix. For
405 this purpose, we (i) cut the column volume by $\frac{3}{4}$, i.e. halving the column diameter to 1 mm, and (ii) tested
406 different quench buffers to potentially shield unspecific binding sites. At this point, we also decided to
407 solely focus on ZrO₂ beads as TiO₂ shows (i) a lower delipidation capacity and (ii) no benefit in terms of
408 unspecific binding on the protein level – the preferred configuration, as lipids are ideally removed pre-
409 digestion to not hamper proteolysis^[36,37]. The smaller phospholipid trap column performs equally efficiently
410 (~99%) in sample delipidation as demonstrated for the bigger column (**Table 1**).

411

412 We applied the following quench buffers: (i) solvent A (0.23% formic acid), (ii) 500 mM glycine-HCl pH
413 2.35, (iii) 5 mg/mL 2,5-Dihydroxybenzoic acid (DHB) in H₂O, (iv) 15 mg/mL DL-lactic acid in H₂O and
414 compared them with the standard quench (100 mM potassium phosphate, pH 2.3) (**Figure S8**). All quench
415 buffers led to a pH of 2.5 upon 1:1 mix (vol/vol) with the standard protein buffer (10 mM potassium
416 phosphate pH 7.0).

417

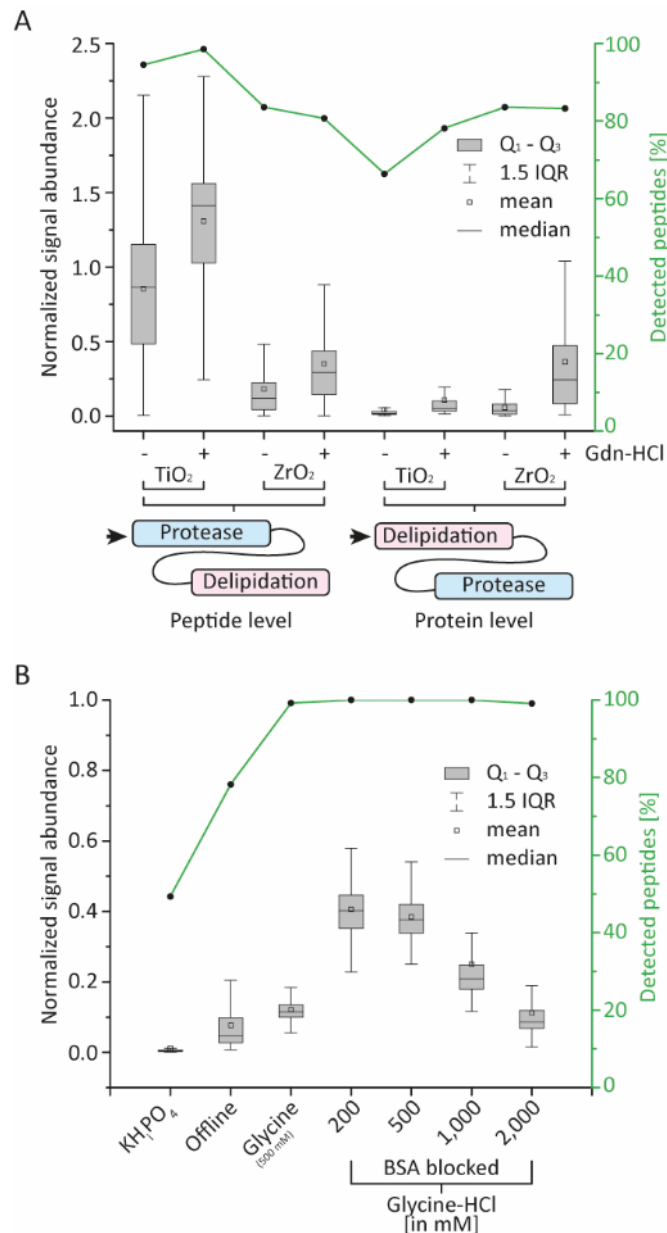
418 DHB and DL-lactic acid were selected as they have previously proven beneficial to prevent unspecific
419 binding in phosphoproteomics^[35,38]. Glycine-HCl was chosen for two reasons. First, it is already known as
420 reliable quench buffer in HDX-MS^[39–41]. Second, amino acids, e.g. arginine, have shown to potentially
421 prevent unspecific protein binding in size exclusion chromatography^[42,43].

422
423 DL-lactic acid exhibits minor but unsatisfactory improvements, while other quench buffers, i.e. solvent A
424 (0.23% formic acid) and DHB, do not lead to any performance gain. The quench buffer of 500 mM glycine-
425 HCl appears to prevent unspecific interaction sites in the ZrO₂ matrix. The average loss of peptide intensity
426 is with roughly one order of magnitude (90%) still high, yet, more importantly, almost 100% of the peptides
427 could be recovered through a sufficient signal-to-noise ratio (**Figure S8**). Quite unexpected though, with
428 an increasing number of technical replicates performed, we observed that the issue of unspecific
429 interactions between protein and ZrO₂ beads became less severe, as evidenced by the obtained
430 chromatograms (**Figure S9**). This phenomenon could be explained by the protein increasingly ‘blocking’
431 unspecific binding sites of the beads. To test whether unspecific protein adsorption could be reduced by
432 protein bead blocking, we prepared a phospholipid ZrO₂ bead trap column blocked with 3% bovine serum
433 albumin (BSA) solubilized in solvent A (0.23% formic acid). BSA is not only a common blocking agent in
434 immunoassays to prevent unspecific protein binding^[44], but has also been applied in combination with ZrO₂
435 beads to obtain robust and reliable results in cell lysis assays^[45]. We then injected PhosB over the blocked
436 and unblocked ZrO₂ phospholipid trap columns using 500 mM glycine-HCl (pH 2.35) as quench buffer.
437 The average peptide signal intensity increases four to five times when ZrO₂ beads are blocked with BSA
438 (**Figure S8**).

439 440 **Optimized Phospholipid Trap Conditions**

441 Finally, we determined the ideal glycine-HCl concentration in the quench buffer. The best performances,
442 measured in terms of peptide signal intensity and identifications, are obtained with 200 and 500 mM glycine-
443 HCl quench buffers, with no significant differences between the two concentrations. To note, the average
444 peptide signal drops at higher concentrated glycine-HCl quench buffers, which might be explained by
445 peptide ion suppression due to incomplete desalting or a detrimental effect on the protein digestion
446 (**Figure 3B**). We then compared the performance of our optimized online delipidation system, in terms of
447 protein recovery, to the off-line ZrO₂-based delipidation protocol proposed in the literature^[10]. Although a
448 higher amount (25 mg) of beads is used to pack the phospholipid trap column in the online system
449 compared to the 10 μ L (3 mg) used in the off-line workflow, in our hands unspecific adsorption in the
450 offline protocol was much higher compared to the automated workflow with glycine-HCl and/or the
451 blockage of the beads (**Figure 3B**). This experiment highlights that this problem requires to be addressed
452 when beads are handled manually (off-line), as reliable measurements are hardly feasible without an
453 adequate strategy to overcome unspecific protein binding. We envision that the BSA-blockage of beads and

454 the use of glycine-HCl as quench buffer will be suitable to prevent protein unspecific adsorption to beads
 455 also in the offline workflow.
 456



457
 458 **Figure 3: Unspecific adsorption of proteins/peptides to the stationary phase of the phospholipid trap**
 459 **column.** (A) Boxplot representing the normalized peptide signal abundance of measurements performed on the
 460 delipidation system relative compared to the standard two-valve HDX-MS configuration. Experiments were
 461 conducted on both protein and peptide level +/- 1.5 M guanidinium-HCl using either a TiO_2 - or a ZrO_2 -based
 462 column. (B) Normalized peptide intensities after applying different glycine-HCl quench buffers w/o BSA bead
 463 blocking in comparison with phosphate buffer (protein level only). Experiments with phosphate buffer were
 464 performed either automated (column-based) or manual after addition of ZrO_2 beads with subsequent filtering of the
 465 sample. The y-axis on the right-hand side (green) indicates the percentage of peptides with sufficiently high signal-to-
 466 noise ratios for reliable peak assignment. IQR \equiv interquartile range. Both glycine-HCl and potassium phosphate (100
 467 mM) quench buffers were mixed 1:1 (vol/vol) with PhosB in 10 mM potassium phosphate, pH 7.0.

468 **Back-exchange and Carry-over**

469 Back-exchange and peptide carry-over are crucial parameters to control in HDX-MS, which can be
470 negatively influenced by an extended flow path and/or an additional column matrix. To investigate the
471 impact of the integrated delipidation system, we conducted PhosB measurements on both configurations
472 and compared back-exchange and carry-over on a large ensemble of peptides (**Figure S10**). For the back-
473 exchange control, we pre-digested PhosB and maximally deuterated the generated peptides with 100% D₂O.
474 While back-exchange levels unsurprisingly vary across peptides, hardly any differences are observed when
475 comparing the same peptide between the two systems (**Figure S10A**). This similitude is also reflected by
476 the calculated average of back-exchange, which accounts for 30.02 ± 0.26 % in the standard two-valve and
477 30.34 ± 0.63 % in the extended three-valve configuration (**Table S9**). The assessment of peptide carry-over
478 also highlights that the delipidation system performs equally well as compared to the standard HDX-MS
479 system, with a total average of 0.77% (85% of all peptides show less than 1% carry-over) for both systems.
480 We also measured PhosB in presence of 1,000 pmol POPC (20 times excess) to investigate whether lipids
481 affect carry-over of hydrophobic peptides. In summary, all peptides show comparable degrees of
482 persistence in both configurations as well as in presence of lipids, which excludes the phospholipid trap
483 column as source of peptide carry-over (**Figure S10B and Table S10**).

484

485

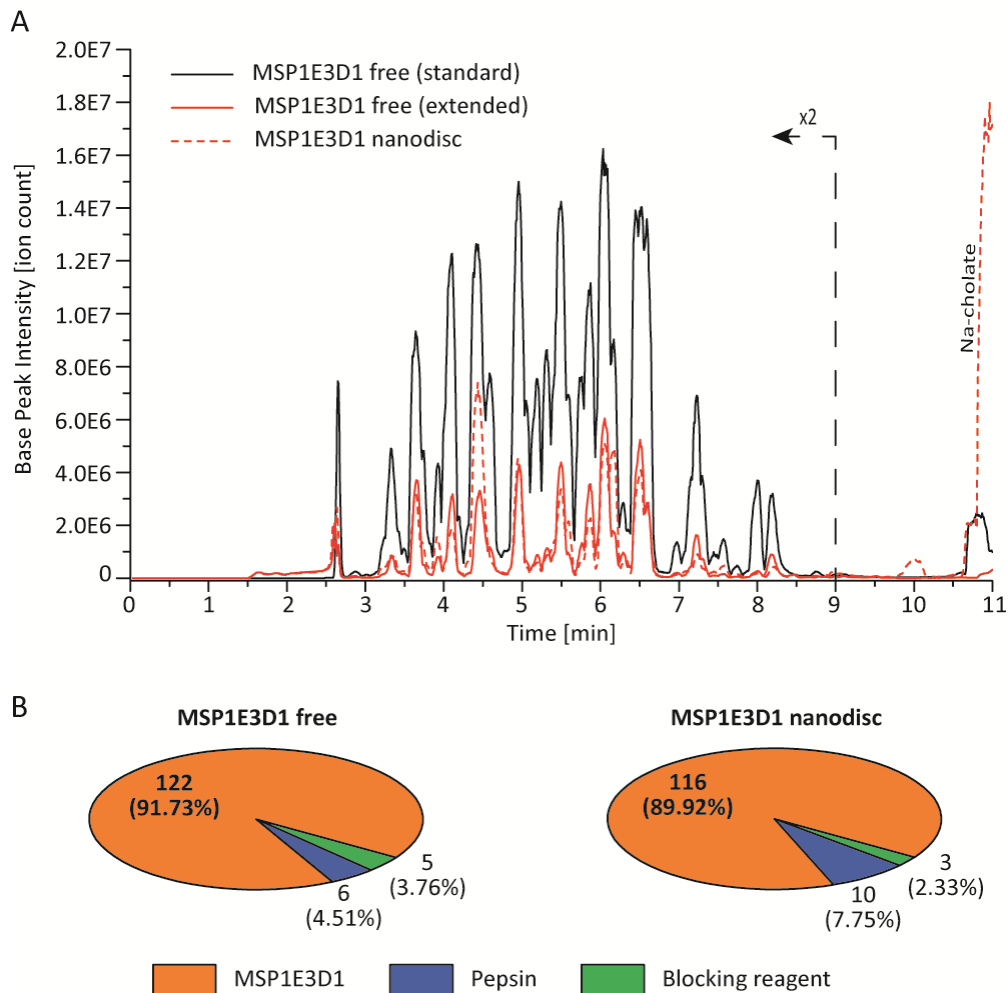
486 HDX-MS Analysis of the Nanodisc Membrane Scaffold Protein using Online Delipidation

487 After optimization, we aimed to test the automated delipidation workflow on nanodisc samples. Nanodiscs
488 utilize a membrane scaffold protein (MSP) – a derivative of apolipoprotein A-1 – capable of encasing an
489 inner lipid core, providing a phospholipid bilayer for membrane protein solubilization^[23,46]. Thus, the MSP
490 protein exists in lipid-free as well as nanodisc form, which makes this type of lipid vesicle an ideal membrane
491 protein system to test the performance of novel HDX-MS workflows.

492

493 First, we measured free MSP1E3D1 – the utilized MSP protein – on the standard two-valve HDX-MS
494 configuration. Subsequently, we applied the extended delipidation configuration to measure MSP1E3D1 in
495 the free as well as nanodisc state (**Figure 4**). The base peak ion chromatogram displays 2-3 x lower
496 intensities when performed on the extended three-valve configuration delipidation system (**Figure 4A**),
497 which is in agreement with previous observations for unspecific protein adsorption under optimized
498 conditions (**Figure 3B**). More importantly, intensities obtained from analysis on the delipidation system
499 both in absence and presence of lipids, i.e. free and nanodisc MSP1E3D1, are of equal magnitude.
500 Furthermore, no differences in the chromatographic profile are present across all chromatograms,
501 indicating that the blocking reagent does not get released over time. For peptide identification we not only
502 targeted MSP1E3D1, but also the blocking protein BSA and the primary digestion reagent pepsin. Free
503 MSP1E3D1 yielded a total number of 122 identified peptides in the two-valve configuration compared to
504 116 peptides obtained for MSP1E3D1 in POPC nanodiscs measured with the three-valve system (**Figure**
505 **4B**). Of interest, the amount of non-MSP1E3D1 peptides account for approximately 10% in both
506 experiments, confirming that the phospholipid trap column is only releasing small quantities of the blocking
507 protein. Full sequence coverage could be obtained for MSP1E3D1 in nanodiscs, measured with the three-
508 valve system (**Figure S11A**) – even slightly better than for free MSP1E3D1 (**Figure S11B**) – demonstrating
509 the functionality of the automated HDX-MS workflow with online delipidation of nanodisc samples.

510



511
512
513
514
515
516
517
518
519

Figure 4: Comparison of MSP1E3D1 (nanodisc) measurements performed on standard two-valve and extended three-valve configuration. (A) Base peak chromatogram of free MSP1E3D1 measured in standard (solid black) and extended (solid red) HDX-MS configuration as well as of nanodisc MSP1E3D1 (dashed red). (B) Number of identified peptides (after filtering with PLGS and DynamX) for the blocking reagent, the protease pepsin, and MSP1E3D1 protein. Peptides identified for each protein species are also reported as a percentage of total peptides identified.

520 Finally, we performed deuterium labeling experiments (ranging from 10 to 10,000 sec) on POPC and EPL
521 nanodiscs as well as on free MSP1E3D1. The deuteration of backbone amide hydrogens in native proteins
522 is mediated by transient opening/closing events in their H-bonding networks^[47,48]. Hence, depending on
523 the rate constants for H-bond opening and closing, two different kinetic regimes can be distinguished for
524 the H/D exchange. When the rate constant for closing (k_{cl}) is much slower ($k_{cl} \ll k_{ch}$) or much faster
525 ($k_{cl} \gg k_{ch}$) than the chemical H/D exchange rate, which is referred to as EX1 and EX2 kinetic, respectively.
526 The EX1 kinetic is characterized by a complete exchange at all backbone amides once unfolding has
527 occurred. Proteins under physiological conditions however tend to follow EX2 kinetic regimes where
528 structural dynamics, i.e. the rate for H-bond closing, is much faster than the chemical H/D exchange rate.
529

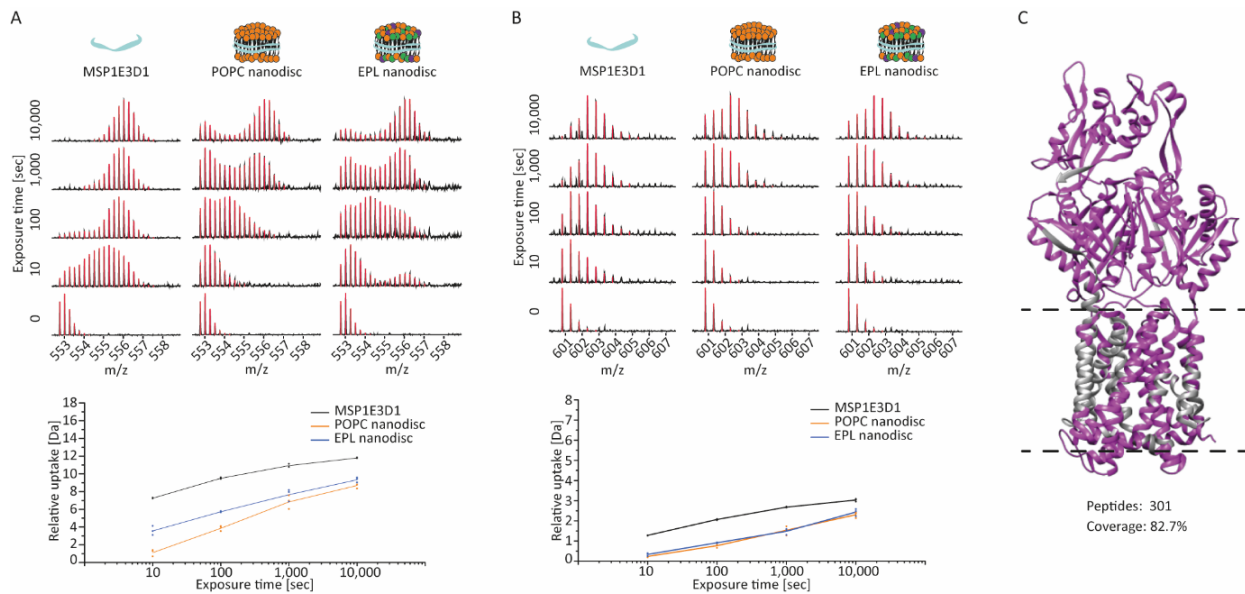
530 We observed that MSP1E3D1 predominantly displays structural dynamics following EX1 kinetic regimes,
531 both in its lipid-free soluble form and when it encases lipids to form nanodiscs (**Figure 5A**). To note, we
532 were able to verify that the isotopic envelope bimodality observed across several peptides of the free
533 MSP1E3D1 does not result from artefacts, e.g peptide carry-over, induced by the three-valve system, as it
534 was observed, and at comparable extent, also for the free form analyzed with the standard two-valve system
535 (**Figure S12**). Importantly, and in line with previous reports^[49], we found that nanodiscs formation leads to
536 stabilization of MSP1E3D1, which is displayed by more intense low-mass envelopes in the EX1 regime of
537 MSP1E3D1 peptides in both nanodiscs forms compared to the soluble form (**Figure 5A, S13**).
538 Furthermore, peptide spectra show significant differences in the evolution of the EX1 kinetics and
539 deuterium uptake for MSP1E3D1 between the two types of nanodiscs, indicating selective modulations of
540 MSP by nanodisc lipids. Lipid-modulated differences are however not always present, as indicated by
541 peptide RTHLAPYLDD (**Figure 5B**).

542

543 Finally, we wanted to test the applicability of the workflow on loaded nanodiscs containing AcrB, a ~115
544 kDa transmembrane protein. We measured AcrB solubilized in POPC nanodiscs under optimized quench
545 conditions and after data processing and peptide filtering, we could obtain 301 peptides and 82.7% sequence
546 coverage (**Figure 5C**), which is higher than previously reported for AcrB in DDM^[26] proving the utility of
547 the established online delipidation setup.

548

549



550

551 **Figure 5: Deuteration of MSP1E3D1 in free, POPC, and EPL nanodisc form.** (A) Stacked spectral plot of
 552 peptide WDNLEKETEGLRQEMSKD (residues 40-57; m/z 552.76; +4) follows an EX1 kinetic regime. The uptake
 553 plot shows a clear difference between both nanodiscs and free MSP1E3D1 indicating a lipid-selective modulation
 554 upon disc formation. A detailed analysis of the different spectra (bimodal fitting) is shown in **Figure S13**. (B) Stacked
 555 spectral plot of peptide RTHLAPYLDD (residues 128-137; m/z 600.80; +2). The uptake plot shows again
 556 stabilization in both nanodiscs. (C) Sequence coverage of AcrB obtained from measurements in POPC nanodisc
 557 (magenta: coverage; grey: no coverage). Dashed lines indicate transmembrane domain.

558

559 **Conclusion**

560 Here, we present an extended HDX-MS system that enables automated sample delipidation for lipid-
561 solubilized membrane proteins. We incorporated a ZrO₂-packed phospholipid trap column online with
562 protein digestion and subsequent peptide analysis. This setup allows phospholipids to be retained in the
563 ZrO₂ matrix of the phospholipid trap column, while proteins pass through and undergo digestion with
564 subsequent peptide trapping. Therefore, the system not only provides an automated but also an economic,
565 and environmentally friendly way of protein delipidation (i.e. reduction of phospholipid trapping beads and
566 plastic usage). We compared ZrO₂ and TiO₂ beads in terms of delipidation efficiency and unspecific
567 protein/peptide binding. ZrO₂ beads have been shown to outperform TiO₂ with delipidation efficiency,
568 which was well above 99% for POPC throughout a course of 30 injections. The efficiency of ZrO₂ beads
569 was also shown to be independent of the type and length of phospholipids, and unlike TiO₂, even capable
570 of retaining Fos-choline-12. We also assessed the level of back-exchange and peptide carry-over for the
571 extended system, verifying that both do not show any noticeable increase compared to the standard HDX-
572 MS configuration.

573
574 The additional column matrix initially led to a significant amount of unspecific protein and peptide binding,
575 which led to unfavourable loss of peptide signals. Minimizing protein loss was a crucial step and required
576 the optimization of both bead and solution conditions. Increasing the amount of protein injected to obtain
577 a sufficiently high MS signal, a strategy commonly applied so far, is unfavorable for two main reasons; i)
578 the increase in sample consumption of the target membrane proteins, which are generally obtained in low
579 amounts due to a challenging expression and purification; and ii) the proportional increase in the amount
580 of lipid components injected, at the expense of their effective removal. We could demonstrate that such
581 protein:bead unspecific adsorption, hence protein loss, can be largely minimized by blocking unspecific
582 binding sites utilizing a combination of blocking reagent, e.g. BSA, and a suitable quench buffer of 200-500
583 mM glycine-HCl, with only a minor effect on lipid removal efficiencies. However, we note that the
584 application of ZrO₂ beads still remains a compromise between delipidation efficiency and the prevention
585 of unspecific protein adsorption. Engineering a different type of beads or a dedicated ZrO₂-based trap
586 column could potentially overcome this issue in future. Furthermore, and more generally, the optimized
587 extended LC setup, equipped with an additional pump, could be utilized to integrate other substrate traps
588 or chromatographic/enzymatic columns into the conventional HDX-MS apparatus, to enhance the
589 flexibility in HDX-MS analysis of complex protein samples.

590
591 Finally, we conducted measurements of MSP nanodiscs to determine the workability of the system. The
592 number of identified peptides of MSP1E3D1 and the sequence coverage map – two crucial metrics in
593 HDX-MS – have demonstrated equal performance compared to control measurements of the free protein,
594 proving the functionality of the developed delipidation setup. Furthermore, we obtained 82.7% sequence
595 coverage of the AcrB membrane protein solubilized in POPC nanodisc, demonstrating the applicability of

596 the system on proteins of interest. This workflow will facilitate membrane protein characterization in HDX-
597 MS to progress our understanding of protein dynamics in lipid environments. Overall, our developments
598 will advance the field of membrane protein structural mass spectrometry, which is now at the point where
599 a lipid milieu must be considered due to its putative relationship with protein structure and function.

600

601

602 **Notes**

603 The authors declare no competing financial interest.

604

605 **Acknowledgments**

606 Work at King's College London by D.H. and E.R. was supported by a UKRI Future Leader Fellowship

607 (MR/S015426/1) to E.R.. C.B. was supported by a King's College London iCASE Studentship with Waters

608 Corporation and B.R.L by a King's College London Studentship. V.C. was supported by the Leverhulme

609 Trust (RPG-2019-178) to A.P, and a King's College London funded research associate position to E.R..

610 A.P. is an EPSRC Research Fellow (EP/V011715/1).

611

612

613

614 **References**

- 615 1. Levental, I. & Lyman, E. Regulation of membrane protein structure and function by their lipid
616 nano-environment. *Nature Reviews Molecular Cell Biology* 2022 1–16 (2022) doi:10.1038/s41580-022-
617 00524-4.
- 618 2. Laganowsky, A. *et al.* Membrane proteins bind lipids selectively to modulate their structure and
619 function. *Nature* **510**, 172–175 (2014).
- 620 3. Yeagle, P. L. Non-covalent binding of membrane lipids to membrane proteins. *Biochimica et*
621 *Biophysica Acta (BBA) - Biomembranes* **1838**, 1548–1559 (2014).
- 622 4. Lee, A. G. Biological membranes: the importance of molecular detail. *Trends Biochem Sci* **36**, 493–
623 500 (2011).
- 624 5. Overduin, M. & Esmaili, M. Memtein: The fundamental unit of membrane-protein structure and
625 function. *Chem Phys Lipids* **218**, 73–84 (2019).
- 626 6. Overington, J. P., Al-Lazikani, B. & Hopkins, A. L. How many drug targets are there? *Nat Rev*
627 *Drug Discov* **5**, 993–996 (2006).
- 628 7. Donnarumma, D. *et al.* Native State Organization of Outer Membrane Porins Unraveled by HDX-
629 MS. *J Proteome Res* **17**, 1794–1800 (2018).
- 630 8. Hansen, R. K., Broadhurst, R. W., Skelton, P. C. & Arkin, I. T. Hydrogen/deuterium exchange of
631 hydrophobic peptides in model membranes by electrospray ionization mass spectrometry. *J Am*
632 *Soc Mass Spectrom* **13**, 1376–1387 (2002).
- 633 9. Redhair, M., Clouser, A. F. & Atkins, W. M. Hydrogen-deuterium exchange mass spectrometry of
634 membrane proteins in lipid nanodiscs. *Chem Phys Lipids* **220**, 14–22 (2019).
- 635 10. Martens, C., Shekhar, M., Lau, A. M., Tajkhorshid, E. & Politis, A. Integrating hydrogen–
636 deuterium exchange mass spectrometry with molecular dynamics simulations to probe lipid-
637 modulated conformational changes in membrane proteins. *Nat Protoc* **14**, 3183–3204 (2019).
- 638 11. Martens, C. *et al.* Direct protein-lipid interactions shape the conformational landscape of
639 secondary transporters. *Nat Commun* **9**, (2018).
- 640 12. Reading, E. Assessing Membrane Protein Structural Dynamics within Lipid Nanodiscs. *Trends*
641 *Biochem Sci* (2019) doi:10.1016/j.tibs.2019.08.003.
- 642 13. Reading, E. *et al.* Interrogating Membrane Protein Conformational Dynamics within Native Lipid
643 Compositions. *Angewandte Chemie* **129**, 15860–15863 (2017).
- 644 14. Reading, E. Structural Mass Spectrometry of Membrane Proteins within Their Native Lipid
645 Environments. *Chemistry - A European Journal* **24**, 13391–13398 (2018).
- 646 15. Masson, G. R. *et al.* Recommendations for performing, interpreting and reporting hydrogen
647 deuterium exchange mass spectrometry (HDX-MS) experiments. *Nat Methods* **16**, 595–602 (2019).
- 648 16. Hebling, C. M. *et al.* Conformational analysis of membrane proteins in phospholipid bilayer
649 nanodiscs by hydrogen exchange mass spectrometry. *Anal Chem* **82**, 5415–5419 (2010).

- 650 17. Walters, B. T., Ricciuti, A., Mayne, L. & Englander, S. W. MINIMIZING BACK EXCHANGE
651 IN THE HYDROGEN EXCHANGE - MASS SPECTROMETRY EXPERIMENT. *J Am Soc*
652 *Mass Spectrom* **23**, 2139 (2012).
- 653 18. Bai, Y., Milne, J. S., Mayne, L. & Englander, S. W. Primary structure effects on peptide group
654 hydrogen exchange. *Proteins: Structure, Function, and Genetics* **17**, 75–86 (1993).
- 655 19. Wales, T. E., Fadgen, K. E., Gerhardt, G. C. & Engen, J. R. High-speed and high-resolution
656 UPLC separation at zero degrees celsius. *Anal Chem* **80**, 6815–6820 (2008).
- 657 20. Iacob, R. E. & Engen, J. R. Hydrogen exchange mass spectrometry: Are we out of the quicksand?
658 *J Am Soc Mass Spectrom* **23**, 1003–1010 (2012).
- 659 21. Anderson, K. W., Gallagher, E. S. & Hudgens, J. W. Automated Removal of Phospholipids from
660 Membrane Proteins for H/D Exchange Mass Spectrometry Workflows. *Anal Chem* **90**, 6409–6412
661 (2018).
- 662 22. Calvaresi, V., Redsted, A., Norais, N. & Rand, K. D. Hydrogen-Deuterium Exchange Mass
663 Spectrometry with Integrated Size-Exclusion Chromatography for Analysis of Complex Protein
664 Samples. *Anal Chem* **93**, 11406–11414 (2021).
- 665 23. Denisov, I. G., Grinkova, Y. v., Lazarides, A. A. & Sligar, S. G. Directed Self-Assembly of
666 Monodisperse Phospholipid Bilayer Nanodiscs with Controlled Size. *J Am Chem Soc* **126**, 3477–
667 3487 (2004).
- 668 24. Denisov, I. G., Baas, B. J., Grinkova, Y. v. & Sligar, S. G. Cooperativity in Cytochrome P450 3A4:
669 LINKAGES IN SUBSTRATE BINDING, SPIN STATE, UNCOUPLING, AND PRODUCT
670 FORMATION. *Journal of Biological Chemistry* **282**, 7066–7076 (2007).
- 671 25. Roos, C. *et al.* Characterization of co-translationally formed nanodisc complexes with small
672 multidrug transporters, proteorhodopsin and with the E. coli MraY translocase. *Biochimica et*
673 *Biophysica Acta (BBA) - Biomembranes* **1818**, 3098–3106 (2012).
- 674 26. Reading, E. *et al.* Perturbed structural dynamics underlie inhibition and altered efflux of the
675 multidrug resistance pump AcrB. *Nature Communications* 2020 11:1 **11**, 1–11 (2020).
- 676 27. Daury, L. *et al.* Tripartite assembly of RND multidrug efflux pumps. *Nature Communications* 2016
677 7:1 **7**, 1–8 (2016).
- 678 28. Guttman, M. *et al.* Tuning a High Transmission Ion Guide to Prevent Gas-Phase Proton
679 Exchange During H/D Exchange MS Analysis. *J Am Soc Mass Spectrom* **27**, 662–668 (2016).
- 680 29. Sørensen, L. & Salbo, R. Optimized Workflow for Selecting Peptides for HDX-MS Data
681 Analyses. *J Am Soc Mass Spectrom* **29**, 2278–2281 (2018).
- 682 30. Guttman, M., Weis, D. D., Engen, J. R. & Lee, K. K. Analysis of overlapped and noisy
683 hydrogen/deuterium exchange mass spectra. *J Am Soc Mass Spectrom* **24**, 1906–1912 (2013).
- 684 31. Aryal, U. K. & Ross, A. R. S. Enrichment and analysis of phosphopeptides under different
685 experimental conditions using titanium dioxide affinity chromatography and mass spectrometry.
686 *Rapid Commun Mass Spectrom* **24**, 219–231 (2010).

- 687 32. Kyono, Y., Sugiyama, N., Imami, K., Tomita, M. & Ishihama, Y. Successive and selective release
688 of phosphorylated peptides captured by hydroxy acid-modified metal oxide chromatography. *J*
689 *Proteome Res* **7**, 4585–4593 (2008).
- 690 33. Simon, E. S., Young, M., Chan, A., Bao, Z. Q. & Andrews, P. C. Improved enrichment strategies
691 for phosphorylated peptides on titanium dioxide using methyl esterification and pH gradient
692 elution. *Anal Biochem* **377**, 234–242 (2008).
- 693 34. Cantin, G. T., Shock, T. R., Sung, K. P., Madhani, H. D. & Yates, J. R. Optimizing TiO₂-based
694 phosphopeptide enrichment for automated multidimensional liquid chromatography coupled to
695 tandem mass spectrometry. *Anal Chem* **79**, 4666–4673 (2007).
- 696 35. Larsen, M. R., Thingholm, T. E., Jensen, O. N., Roepstorff, P. & Jørgensen, T. J. D. Highly
697 Selective Enrichment of Phosphorylated Peptides from Peptide Mixtures Using Titanium Dioxide
698 Microcolumns. *Molecular & Cellular Proteomics* **4**, 873–886 (2005).
- 699 36. Calvaresi, V. *et al.* Conformational dynamics of free and membrane-bound human Hsp70 in
700 model cytosolic and endo-lysosomal environments. *Communications Biology* **2021 4:1** **4**, 1–11 (2021).
- 701 37. Burke, J. E. *et al.* Interaction of group IA phospholipase A2 with metal ions and phospholipid
702 vesicles probed with deuterium exchange mass spectrometry. *Biochemistry* **47**, 6451–6459 (2008).
- 703 38. Sugiyama, N. *et al.* Phosphopeptide enrichment by aliphatic hydroxy acid-modified metal oxide
704 chromatography for nano-LC-MS/MS in proteomics applications. *Molecular and Cellular Proteomics*
705 **6**, 1103–1109 (2007).
- 706 39. Comamala, G. *et al.* Hydrogen/Deuterium Exchange Mass Spectrometry with Integrated
707 Electrochemical Reduction and Microchip-Enabled Deglycosylation for Epitope Mapping of
708 Heavily Glycosylated and Disulfide-Bonded Proteins. *Anal Chem* **93**, 16330–16340 (2021).
- 709 40. Rey, M. *et al.* Effective removal of nonionic detergents in protein mass spectrometry,
710 hydrogen/deuterium exchange, and proteomics. *Anal Chem* **82**, 5107–5116 (2010).
- 711 41. Soya, N., Roldan, A. & Lukacs, G. L. Differential Scanning Fluorimetry and Hydrogen Deuterium
712 Exchange Mass Spectrometry to Monitor the Conformational Dynamics of NBD1 in Cystic
713 Fibrosis. *Methods Mol Biol* **1873**, 53–67 (2019).
- 714 42. Yumioka, R., Sato, H., Tomizawa, H., Yamasaki, Y. & Ejima, D. Mobile phase containing arginine
715 provides more reliable SEC condition for aggregation analysis. *J Pharm Sci* **99**, 618–620 (2010).
- 716 43. Ejima, D., Yumioka, R., Arakawa, T. & Tsumoto, K. Arginine as an effective additive in gel
717 permeation chromatography. *J Chromatogr A* **1094**, 49–55 (2005).
- 718 44. Hasui, K. & Murata, F. A new simplified catalyzed signal amplification system for minimizing
719 non-specific staining in tissues with supersensitive immunohistochemistry. *Arch Histol Cytol* **68**, 1–
720 17 (2005).
- 721 45. Vandeventer, P. E. *et al.* Mechanical Disruption of Lysis-Resistant Bacterial Cells by Use of a
722 Miniature, Low-Power, Disposable Device. *J Clin Microbiol* **49**, 2533–2539 (2011).

- 723 46. Bayburt, T. H., Grinkova, Y. v. & Sligar, S. G. Self-Assembly of Discoidal Phospholipid Bilayer
724 Nanoparticles with Membrane Scaffold Proteins. *Nano Lett* **2**, 853–856 (2002).
- 725 47. Konermann, L., Tong, X. & Pan, Y. Protein structure and dynamics studied by mass
726 spectrometry: H/D exchange, hydroxyl radical labeling, and related approaches. *Journal of Mass*
727 *Spectrometry* **43**, 1021–1036 (2008).
- 728 48. Hvidt, A. & Nielsen, S. O. Hydrogen Exchange in Proteins. *Adv Protein Chem* **21**, 287–386 (1966).
- 729 49. Morgan, C. R. *et al.* Conformational transitions in the membrane scaffold protein of phospholipid
730 bilayer nanodiscs. *Molecular and Cellular Proteomics* **10**, (2011).

731

732

733